[1]

Improved Lunar Intrusion Detection Algorithm for the CrIS Sensor Data Record

Yong Chen, Denis Tremblay, Likun Wang, Flavio Iturbide-Sanchez

***Abstract*—As one of the calibration reference targets used to calibrate the Cross-track Infrared Sounder (CrIS) Earth scene (ES) measurements, the stable deep space (DS) reference spectrum in the 30-scan DS calibration moving window is very important for the accuracy of the calibrated ES radiances. The DS view changes when the lunar radiation intrudes into the observation field of view (FOV). In the original CrIS lunar intrusion (LI) detection algorithm implemented in the operational ground processing system, the contaminated DS spectra were not effectively removed from the DS moving window due to large threshold values and the assumption that the first DS spectrum in the moving window was not contaminated. As a result, inaccurate, degraded, or invalid ES radiances were produced in the operational CrIS Sensor Data Record (SDR) during lunar intrusion events. In this study, an improved LI detection algorithm is developed and implemented into the operational system. First, the new algorithm efficiently finds a contamination-free DS spectrum in the DS 30-scan calibration moving window to use as the reference spectrum. Second, based on the phase characteristics of the complex raw DS spectra during LI events, the lunar intrusion band-dependent thresholds were derived to effectively reject the contaminated DS spectra and make the valid DS window size consistent among the three CrIS bands. The new LI algorithm implemented in the operational system shows a successful detection and removal of all the lunar-contaminated DS spectra in the DS moving window, resulting in improved ES radiances calibration during LI events.**

***Index Terms*—CrIS, Calibration, Lunar intrusion detection, Contamination, Moving window**

I. Introduction

THE Cross-Track Infrared Sounder (CrIS) is a Fourier transform spectrometer (FTS), currently on board the Suomi National Polar-Orbiting Partnership (S-NPP) and NOAA-20 satellites. S-NPP was launched on 28 October 2011, while NOAA-20 was launched on 18 November 2017. The CrIS ground processing software Interface Data Processing Segment (IDPS), part of the Joint Polar Satellite System (JPSS) ground processing system, transforms the measured raw interferograms (raw data record, RDR) into calibrated and geolocated spectra in the form of Sensor Data Records (SDRs). The SDRs cover three spectral bands: the long-wave IR (LWIR) band from 650 to 1095 cm^{-1}, mid-wave IR (MWIR) band 1210 to 1750 cm^{-1}, and short-wave IR (SWIR) band 2155 to 2550 cm-1 with nominal spectral resolutions (NSR) of 0.625 cm^{-1}, 1.25 cm^{-1}, and 2.5 cm^{-1}, respectively. CrIS also provides full spectral resolution (FSR) SDR with spectral resolution of 0.625 cm^{-1} for all three bands since 4 December 2014. For one 8-second scan, CrIS sequentially measures 34 interferogram sweeps or field of regards (FORs) with a 3 × 3 array of field of views (FOVs), including 30 Earth scene (ES), 2 deep space (DS), and 2 Internal Calibration Target (ICT) measurements. Among them, half of the ES, DS, and ICT interferograms are measured in a forward direction and the other half in the reverse direction according to the moving direction of interferometer porchswing mirror. Radiometric calibrations are performed separately for different sweeping directions, FOVs, and bands using ICT and DS measurements as calibration references.

CrIS is a well-calibrated instrument characterized with its unique instrument design and well-conducted pre-launch and post-launch validations. The high quality of CrIS observations is found on its low radiometric noise (well below specifications), high spectral, radiometric and high geolocation accuracy, demonstrated over long-term and with high stability [1-9]. Recent studies demonstrated that the CrIS SDR data meet calibration requirements (see Table 2 in [1]), making them an exceptional asset not only for weather applications [10] but also for climate applications [11]. CrIS SDRs for S-NPP and NOAA-20 reached the validated status on 20 February 2014 and 2 October 2018, respectively.

In CrIS operational SDR radiance products, lunar intrusion is identified by one dedicated lunar intrusion quality flag variable called Quality Flag 2 (QF2) [12], which specifically indicates that some of the DS views in the DS calibration moving window are contaminated by lunar radiation. After the launch of the S-NPP and NOAA-20 satellites into orbit, it was observed that the LI happened several times a year and each time lasts several consecutive orbits as shown in Fig. 1. The lunar-contaminated DS view measurement can seriously affect the Earth scene calibration accuracy if it is not effectively

[1]Manuscript received May 2019; revised August 2019; accepted September 2019. This work was supported by the National Oceanic and Atmospheric Administration under contract ST133017CQ0050. The contents of this paper are solely the opinions of the authors and do not constitute a statement of policy, decision, or position on behalf of NOAA or the U. S. Government.

Y. Chen and D. Tremblay are with Global Science and Technology, Inc., 7855 Walker Derive, Suite 200, Greenbelt, MD 20770 USA (e-mail: Yong.Chen@noaa.gov, Denis.Tremblay@noaa.gov).

L. Wang is with Riverside Technology, Inc., 1100 Bonifant Street, Suite 240, Silver Spring, MD 20910 USA (email: Likun.Wang@noaa.gov)

F. Iturbide-Sanchez (IEEE Senior Member) is with the Center for Satellite Applications and Research, National Environmental Satellite, Data, and Information Service (NESDIS), National Oceanic and Atmospheric Administration, College Park, 20740, USA (e-mail: Flavio.Iturbide@noaa.gov)

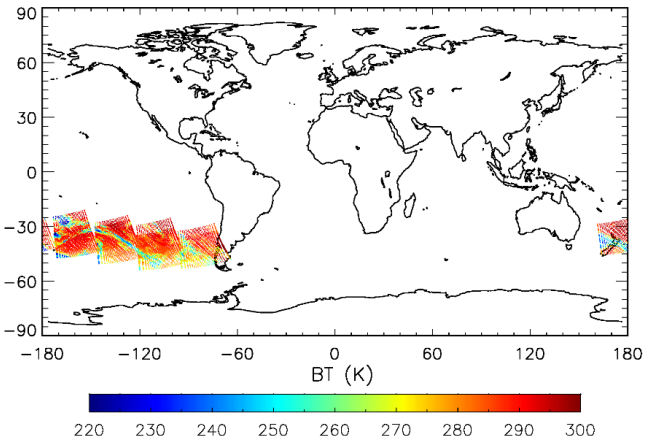

Fig. 1. Global distribution and brightness temperature at 900 cm^{-1} for lunar intrusion events on 25 and 26 February 2018 indicated by the quality flag QF2 in the operational S-NPP SDR data product.

detected and removed. Due to the issues of the original lunar detection algorithm in the IDPS, there were noticeable ES radiance changes during these LI events, particularly for LWIR and MWIR bands, without triggering the overall data quality flag. In some cases, degraded and invalid ES radiances occurred, especially for SWIR band.

Focused on improving the lunar intrusion detection algorithm, this study has the major purpose to remove the DS spectra contaminated by lunar contribution in the DS calibration moving window, and thus to improve the quality of ES radiances during lunar intrusion events. The improved radiometric accuracy and improved ability to flag bad spectra in overall quality flag during lunar intrusion events will generate higher-quality CrIS SDR and downstream products. The new LI detection algorithm includes two major improvements compared to the original one: 1) to find the baseline DS reference spectrum without contamination in the DS calibration moving window, and 2) to use optimal thresholds for three CrIS bands to effectively reject the contaminated DS spectra and to make the valid DS window size consistent among the three bands.

The paper is organized as follows. Section II describes the original algorithm that was used to detect the lunar contamination. A new and improved algorithm is then developed in Section III. The impacts of removing the lunar-contaminated DS spectra on the improvements of CrIS calibrated ES radiances are presented in Section IV. Conclusion is given in Section V.

II. Original Lunar Detection Algorithm: Discussion and Identified Limitations

The Earth scene measurements are calibrated radiometrically with two known reference targets: the ambient blackbody ICT (nominal temperature at 280 K), and the DS view (whose external radiance contribution is negligible). To calibrate the ES spectra at the N scan, N-15 to N+14 (total 30) consecutive ICT and DS raw spectra in the moving window are averaged to increase the calibration stability. Following [13], the uncalibrated complex spectrum in digital unit (C) is the sum of the two terms, one from the viewing external source and the other from the internal emission of the instrument. The two terms have different phases: external phase ϕ_{ex}, and internal phase ϕ_{in}:

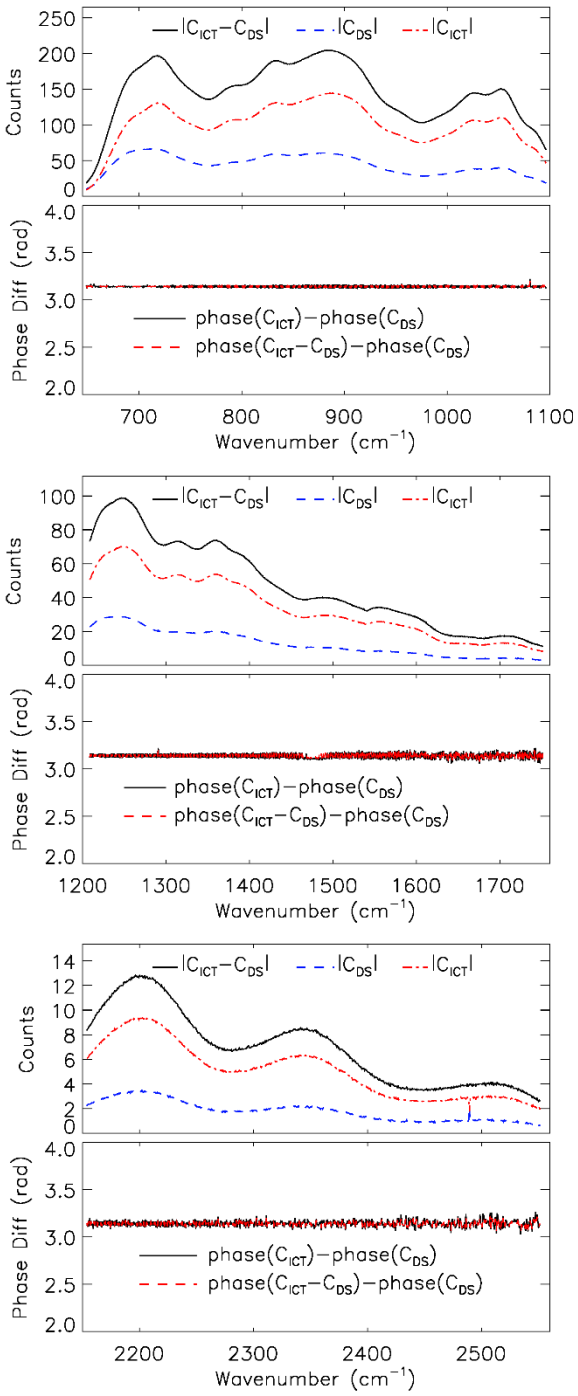

Fig. 2. Magnitudes of the FOV 1 raw spectra $C_{ICT} - C_{DS}$ (solid black curve), C_{DS} (dashed curve), and C_{ICT} (dot-dash curve), and phase differences between C_{ICT} and C_{DS} (solid black curve) and between $C_{ICT} - C_{DS}$ and C_{DS} (dashed curve), both of which are very close to π for all three CrIS bands.

$$C = A_{ex}e^{i\Phi_{ex}} + A_{in}e^{i\Phi_{in}} \quad (1)$$

where A_{ex} and A_{in} are the magnitude of the external source and instrument emission, respectively. The CrIS instrument emission term is nearly 180° out of phase with respect to the phase of the external source due to the mirror reflection. Following this model, the raw spectra from ICT and DS are expressed as

$$C_{DS} = A_{moon}e^{i\Phi_{ex}} + A_{in}e^{i\Phi_{in}}, \quad (2)$$

$$C_{ICT} = A_{ICT}e^{i\Phi_{ex}} + A_{in}e^{i\Phi_{in}} \quad (3)$$

where A_{moon} is the magnitude of the Moon radiation contribution when the Moon is in the DS view. Under normal conditions, the DS spectrum is not contaminated by external radiation sources, and the measured radiation from the DS external observation is effectively zero. Figure 2 shows an example of the magnitudes of measured ICT and DS raw spectra and phase for three CrIS bands (LWIR, MWIR, and SWIR) at FOV1 under normal conditions. One can see that magnitudes of $|C_{ICT} - C_{DS}|$ (solid black curve) is larger than both $|C_{DS}|$ (dashed curve) and $|C_{ICT}|$ (dot-dash curve), and the phase differences between C_{ICT} and C_{DS} (solid black curve) and between $C_{ICT} - C_{DS}$ and C_{DS} (dashed curve) are very close to π for all three CrIS bands. One can also see that the highest instrument response regions are located at [864 cm^{-1}, 901 cm^{-1}], [1234 cm^{-1}, 1271 cm^{-1}], and [2184 cm^{-1}, 2222 cm^{-1}] for CrIS LWIR, MWIR, and SWIR, respectively. These channels will be used in the new lunar intrusion algorithm to find the non-lunar-contaminated DS spectrum in the moving window.

The potential lunar-contaminated DS signal can be identified using a simple model based on the CrIS DS viewing angle. The DS viewing angle measured from the satellite nadir is 70.3° with ±0.04° uncertainty. The LI happens only when the separation angle between the DS vector and the lunar vector are less than a certain values. Using the Naval Observatory Vector Astrometry Software (NOVAS) version 3.1 (providing community standard transformation between the terrestrial and celestial coordinate systems) [14], the Jet Propulsion Laboratory Solar System Ephemeris (providing Sun and Moon ephemeris) [15], as well as Simplified General Perturbation model SGP4 (predicting orbit propagator) [16], two vectors can be calculated: CrIS DS exit vector (or line-of-sight) in the Earth Centered Inertial (ECI) frame (LOSVect) and lunar vector in ECI frame (LunarVect). By knowing the separation angle between the two vectors one can conclude the following: if it less than CrIS FOR aperture angle 3.3°, (or FOV aperture angle 0.963°), then the Moon is in CrIS FOR (or FOV). Figure 3 shows an example of potential lunar events during 2018. When the Moon was in the CrIS FOR, the red curve (the separation angle between the CrIS space view and Moon vectors) is below the black line (CrIS FOR angle 3.3°). The lunar intrusion occurs about every ~29.3 days, except in summer between August and October as found in Fig.3. In addition, the lunar phase angles (blue curve) have limited dynamic ranges between 50° to 90° when LI occurs.

In the CrIS SDR radiance products, there are several assessments of the quality of DS spectra, including data quality indicators (DQI) and data quality flags (DQF) [12]. DS calibration window size (DS_WindowSize) and DS spectral stability (DS_SpectralStability) are two DQIs to monitor the DS spectra quality. DS_WindowSize is used to record how many DS spectra are averaged to obtain the DS reference spectrum in the moving window and to calibrate the corresponding ES spectra with dimension 2 sweep directions × 9 FOVs × 3 bands.

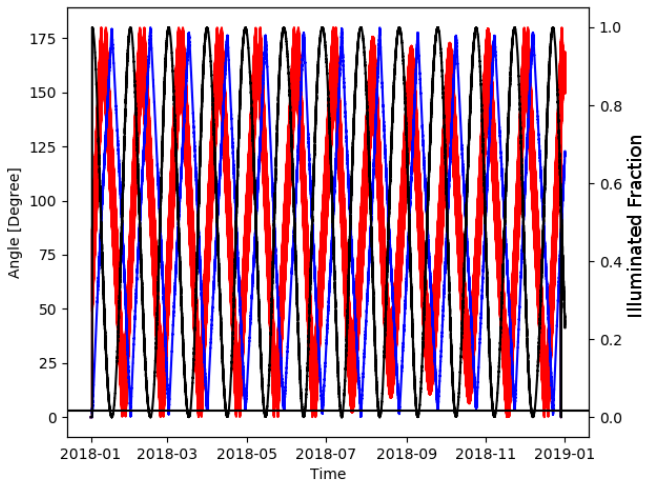

Fig. 3. Moon in CrIS field of regard during 2018. Red curve-separation angle between the CrIS space view and the Moon vector; Blue curve-separation angle between the Sun and the Moon vectors as lunar phase; Black curve-Moon illuminated fraction; and Black line-CrIS FOR angle (3.3°).

The DS_WindowSize will be less than 30 if there is any rejection to the DS spectra in the moving window. The DS_SpectralStability has the same dimension as DS_WindowSize and is used to monitor the spectral variability of DS view spectra within the DS moving window. It is calculated using the following equation:

$$DS\_SpectraStability = \frac{1}{N}\sum_{i=1}^{N}\sigma(i)$$

where N is the number of spectral bins, $\sigma(i)$ is the standard deviation of the DS spectral count magnitude in the ith bin over the data samples (DS_WindowSize) within the moving window. There is one dedicated lunar intrusion quality flag (QF2) to specifically indicate the lunar intrusion occurrence with dimension 9 FOVs × 3 bands. This quality flag QF2 is an 8-bit integer variable. The first bit is used for the forward sweep direction, while the second bit is for the reverse sweep direction. The bit is set accordingly when there are at least one or more DS view measurements is affected by the Moon in the set of DS measurements within the 30-scan moving window when the porchswing mirror has a forward or reverse sweep direction. When the lunar intrusion algorithm detects a lunar-contaminated DS spectrum based on the prescribed threshold, the DS spectrum then is removed from the DS moving window, resulting in smaller DS window size (less

than 30) and setting QF2. When some lunar-contaminated DS spectra were not effectively removed from the 30-scan moving window, then DS_SpectralStability will show larger variability as a function of scans. When DS_WindowSize is less than 15, the overall quality flag (QF3) will be set to "degraded", to indicate that the corresponding ES radiance spectra may have some issues due to the DS calibration averaging becoming less representative of the instrument background around the Earth scene measurement. Under some extreme conditions, the undetected lunar-contaminated DS spectra in the 30-scan moving window may introduce a significant error of the computed DS reference spectrum. The calibrated ES radiance using the contaminated DS reference spectrum may be impacted. This usually results in larger imaginary part of the ES spectra, exceeding thresholds and QF3 set to invalid by the SDR quality control algorithm.

The steps for the original lunar intrusion detection algorithm [17] are summarized below:

1) Given the newest DS spectrum that was not included in the current uncalibrated averaged DS spectrum in the moving window (referred as reference DS spectrum), the difference between the new DS spectrum and the average DS spectrum (denoted by operator < >) at each wavenumber bin "n" for each band "b", FOV "p" and sweep direction "d" can be obtained by

$$R^{ds}_{b,p,d}[n] = C^{ds}_{b,p,d}[n] - \langle C^{ds}_{b,p,d}[n] \rangle \quad (4)$$

2) The difference between the averaged uncalibarated ICT spectrum (reference ICT spectrum) and reference DS spectrum in the moving window is given by

$$R^{ict}_{b,p,d}[n] = \langle C^{ict}_{b,p,d}[n] \rangle - \langle C^{ds}_{b,p,d}[n] \rangle \quad (5)$$

3) Compute the mean value of the real part of the $R^{ds}_{b,p,d}[n]$ value (difference between the new and average DS spectrum), relative to the background-subtracted ICT spectrum ($R^{ict}_{b,p,d}[n]$) over a CrIS band, and compare it to a configurable LI threshold (currently set to 0.1 for three CrIS bands),

$$\frac{\sum_{n_{min}}^{n_{max}} Re\left(\frac{R^{ds}_{b,p,d}[n]}{R^{ict}_{b,p,d}[n]}\right)}{n_{max} - n_{min}} > LI_{lim} \quad (6)$$

where n_{min}, and n_{max} are the wavenumber bins corresponding to the lower and upper band edge, respectively. In the original algorithm, the DS moving window is established as following: The valid DS spectra are added sequentially into the moving window, the DS reference spectrum is calculated by averaging these valid DS spectra in the moving window. At the beginning of the data processing initialization, the first DS spectrum is pushed into the moving window as the reference spectrum. The lunar intrusion detection algorithm is used to detect and reject any subsequent lunar-contaminated DS spectra.

On March 8, 2018, there was a major configuration change in the IDPS system when it was transitioned from Block 1 to Block 2 version. Block 2 was designed to process both S-NPP and NOAA-20, while Block 1 version can only process S-NPP. Before IDPS Block 2 became operational, no degraded or invalid ES view spectra was detected during the lunar intrusion events. However, it was found that the DS_SpectralStability had larger variation as a function of scans during the LI events. This indicated that the lunar-contaminated DS spectra were included in the calculation of the DS reference spectrum. After 8 March 2017, LI events caused degraded and invalided ES radiances, especially in SWIR band, for cases when the DS view moving window was less than 15, except for August, September and October due to the CrIS view geometry (see Fig. 3). In order to reduce the operational SDR latency, in Block 2 it was decided to switch from a single process to multiple processes. After Block 2 was implemented, the original CrIS lunar intrusion detection algorithm in the operational code started having problems associated with the multiple processes running with parallel setting, since it requires the DS 30-scan moving window to be reestablished for each process. For example, when the first DS spectrum is contaminated by the Moon, those valid and normal deep space spectra sequentially added into the moving window are rejected. This condition generates very small DS window size (less than 15), resulting in a contaminated and distorted DS reference spectrum and degraded/invalid calibrated earth view spectra. The detection threshold is originally set to a very large value of 0.1, which represents the maximum allowable increase of the DS spectral count relative to the ICT spectrum for all three bands. In summary, the original LI detection algorithm cannot effectively reject the contaminated deep space views from the DS moving window, produces larger radiometric errors in the calibration of the ES spectra, results in inconsistent valid DS window sizes for all three bands, and makes the DS spectral stability inconsistent as a function of scan lines.

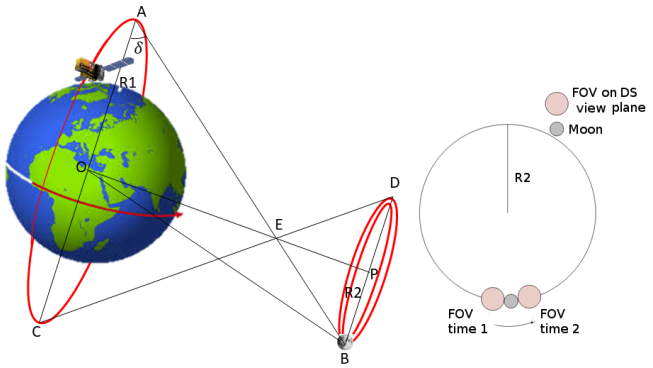

Fig. 4. Scheme of the lunar intrusions in CrIS deep space view plane in which the Moon's position falls on the circle to derive the number of successive DS view affected by a single lunar intrusion event.

III. Improved Lunar Intrusion Detection Algorithm

A. Maximum Number of Lunar Contaminated DS Spectra

It is very important to know theoretically how many DS spectra for a given CrIS FOV are affected by the lunar

radiation over the full duration of a lunar intrusion event. For this purpose, Figure 4 is used to show the number of lunar-contaminated DS views for a single FOV. Neglecting the spacecraft orbital eccentricity, variation of space attitude in the orbital frame, and the Moon motion, it is observed that the S-NPP or NOAA-20 orbit plane, with point O as a center, and the space view plane for the Moon, with point P as a center, are two parallel planes. The space view angle δ for CrIS sensor is located at 70.3° from the satellite nadir. R_2 is the radius in the space view plane in which the Moon's position fall on the circle when lunar intrusion occurs (left panel in Fig. 4). *OB* is the Earth-moon mean distance, while R_1 is the nominal satellite height plus the Earth mean radius. AB is the distance between the CrIS sensor and the Moon, and E is the intercept point between AB and OP. The maximum number of scans with successive DS views that is possible in a single LI event, N_{LI}, is about 10.3. This number can be derived based on the Moon moving in and moving out the CrIS FOV at the space view plane (see right panel in Fig. 4) using the following equations:

$$OB^2 = R_1^2 + AB^2 - 2 \cdot R_1 \cdot AB \cdot \cos\delta \tag{7}$$

$$AE = R_1 / \cos\delta \tag{8}$$

$$R_2 = R_1 \bullet \frac{(AB-AE)}{AE} \tag{9}$$

$$N_{LI} = \frac{D_{moon}+D_{FOV}}{2\pi \cdot R_2} \bullet \frac{T_{orbit}}{T_{scan}} \approx 10.3 \tag{10}$$

where D_{moon} is the mean diameter of the Moon, and D_{FOV} is the apparent CrIS FOV diameter at the DS view plane: AB times CrIS FOV detector diameter (0.016808 radians). T_{orbit} is the orbit period and T_{scan} is the time for one scan. The distance OB corresponds to the Moon center closest distance to the Earth center at its orbital perigee. For CrIS, the periods are about 6086 seconds, and 8 seconds for one orbit and one scan, respectively.

B. Impact of Lunar Radiation Contribution to the DS View

In a lunar intrusion event, the DS spectra go through a process of the Moon moving in and out of the FOV. The DS spectrum (C_{DS}) varies from one component (instrument emission only) to two components when the Moon moves into the FOV and then to one component again after the Moon move out of the FOV, as depicted in (2). Figure 5 shows the time evolution of the real part (solid black curve) and imaginary part (dashed blue curve) of the DS spectrum C_{DS}, as well as its phase (red curve with solid circle) at (a) wavenumbers 882.5 cm^{-1} from LWIR band, (b) 1252.50 cm^{-1} from MWIR band, and (c) 2203.125 cm^{-1} from SWIR band for S-NPP CrIS FOV 1 reverse mirror sweep direction on 25 February 2018 during a lunar intrusion event. The time information is provided by the scan number in the day with the interval of 8 seconds between two adjacent scans. It can be seen that during this event, the Moon moves into the CrIS FOV at the scan 9496 and moves out at the scan 9505. Since the lunar radiation component has a phase differing from the instrument emission component by about π, the magnitude of C_{DS} decreased as the Moon moves in. This effect is found when observing how the real and imaginary parts of C_{DS} move toward and cross the zero count values, as shown in the Fig. 5 (b) and 5(c) for the MWIR and SWIR channels. If the measurement is taking fast enough, there could be a C_{DS} (in between scans 9496 and 9497, and between scans 9503 and 9504) whose value is zero. Between these two zero count points at which the real and imaginary parts cross, the lunar radiation component is larger than the instrument emission and the spectrum C_{DS} has a phase that differs by almost a π from that when the Moon is not in the FOV. For the LWIR channel shown in Fig. 5(a), the lunar radiation component is less than the instrument emission. The real and imaginary parts do not cross at all and do not reach the zero count values, as a result, the phase only shifts a very small amount (less than 0.2 radian) compared to about a π as seen in Fig. 5(b) and 5(c). In a relative term, the SWIR channels are more sensitive to the lunar radiation component contribution than for the LWIR and MWIR channels due to higher electronic amplification and the lunar spectrum characteristics.

C. Determination of the Lunar Intrusion Thresholds

To derive the LI thresholds for three CrIS bands and to improve the LI detection algorithm, ICT and DS raw spectra data from lunar intrusion events were collected since the launch of both S-NPP and NOAA-20. Since the maximum number of lunar-contaminated DS spectra does not exceed 10 consecutive

(a) DS count and phase at wavenumbers 882.5 cm^{-1} from LWIR band

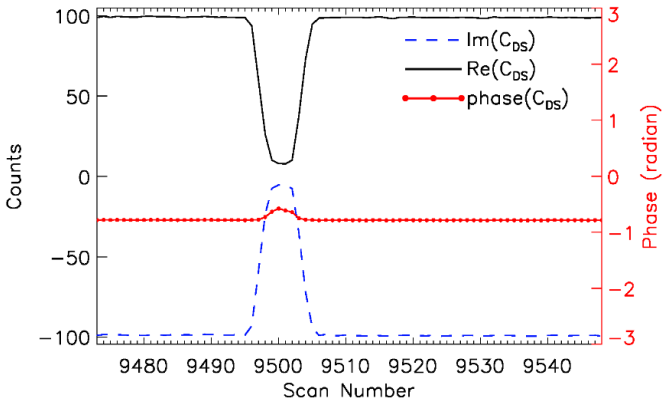

(b) DS count and phase at wavenumber 1252.50 cm^{-1} from MWIR band

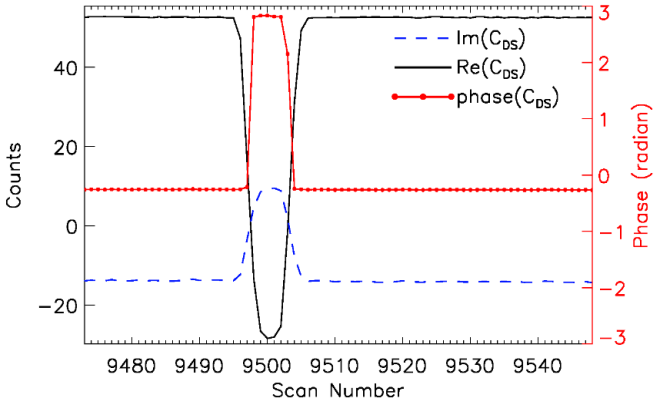

(c) DS count and phase at wavenumber 2203.125 cm^{-1} from SWIR band

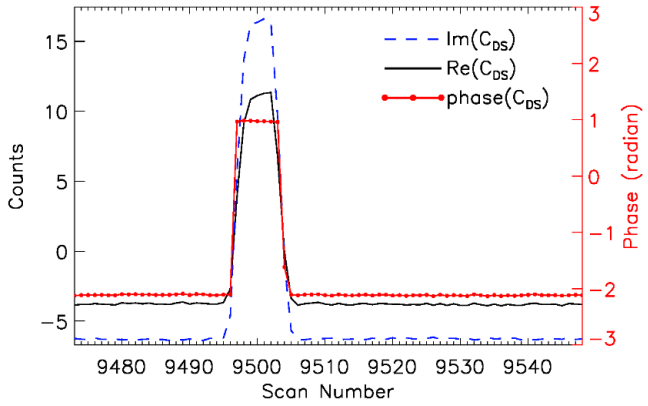

Fig. 5. Time series of S-NPP CrIS FOV 1 reverse interferometer sweep direction DS count at (a) wavenumbers 882.5 cm^{-1} from LWIR band, (b) 1252.50 cm^{-1} from MWIR band, and (c) 2203.125 cm^{-1} from SWIR band on 25 February 2018 during a lunar intrusion event. Solid black curve-real part; dashed blue curve-imaginary part; connected solid circle-phase. The time scale is represented by the scan number stepping (8 seconds per scan) with a period of 10 minute 8 seconds. The Moon moves in the FOV at scan number 9496 and moves out at scan number 9505. The lunar intrusion introduces an absolute phase change close to π at scan numbers 9497 and 9503 in the MWIR and SWIR bands.

scans for a given FOV in one lunar intrusion event, after removing the lunar-contaminated DS spectra from the DS moving window, there are still having enough valid DS spectra (not less than 20) to calculate the reference DS spectrum. As a result, the calibrated SDR data products should have high data quality, since the size of DS window is usually greater than 15 during any lunar intrusion event. Based on the phase impact of lunar radiation contribution to the DS spectrum, the scan positions for the lunar-contaminated DS spectra can be identified using the SWIR channels. The same positions can also be used for MWIR and LWIR since CrIS observes the same DS scene for all three spectral bands. Based on (6), the DS spectral variation is defined as in (11)

$$V^{ds}_{b,p,d} = \frac{\sum_{n_{min}}^{n_{max}} Re\left(\frac{R^{ds}_{b,p,d}[n]}{R^{ict}_{b,p,d}[n]}\right)}{n_{max} - n_{min}} \quad (11)$$

This parameter is used to quantify DS spectral variability. To derive this parameter, the lunar-contaminated DS spectra are excluded from the DS moving window and the reference DS spectrum is only derived from the normal DS spectra. This variable can effectively evaluate the impact of lunar-contaminated DS spectra compared to the normal DS spectra. Together with the phase information, optimal band-dependent thresholds can be determined. Using the 25 February 2018 lunar event as an example, the DS spectral variation was computed and shown in Fig. 6. In this lunar intrusion event, FOVs 1 (black curve), 2 (blue curve), 5 (green curve), and 6 (red curve) have lunar-contaminated DS views from scan 9496 to scan 9521. The three bands for each FOV are distinguished by using different symbols in the curves. Filled circle is for SWIR, open square for MWIR, and open triangle for LWIR. One can see that the DS spectral variation from the three bands have different responses. DS spectral variation from SWIR is the strongest, can reach to about 2.5. DS spectral variation from MWIR is weaker than SWIR, but stronger than LWIR, the largest value can be around 1.0. The DS spectral variation from LWIR is the weakest, only around 0.5. This feature is very consistent with the DS phase changes shown in Fig. 5. Two neighboring FOVs can observe the lunar-contaminated DS scenes simultaneously at the same scan, for example, FOVs 1 and 2 at scan 9505, and FOVs 2 and 5 at scans 9507 to 9511.

An optimal lunar intrusion threshold should: 1) help to effectively reject the contaminated deep space views, in order to minimize radiometric errors, 2) help to make the valid DS window size the same among different bands, and 3) help to make the DS spectral stability consistent as a function of scan lines. The DS spectral stability is a well-founded metric to indicate the presence of lunar contaminated DS spectra in the DS moving window. In the operational lunar intrusion algorithm, the LI_{lim} values are set to 0.1 for the three bands. It has been found that this threshold is suboptimal and very loose, causing large variability in the DS spectral stability for all three bands, when contaminated DS spectra are included in the DS reference spectrum. This performance is discussed with more detail in Results Section IV). Based on Fig. 6, Figure 7 illustrates the changes of the DS spectral variation as a function of scans during the lunar intrusion event. From Fig. 7, one can identify that the SWIR have larger DS variations in comparison to those observed over the MWIR and LWIR bands. Typical SWIR DS variations are around ±0.002, while variations from MWIR and LWIR bands are less than 0.001. For FOV 1 (black curves with different symbols), starting from scan 9495, the DS variations begin to rise to around 0.002, 0.0025, and 0.0045 at LWIR, MWIR and SWIR, respectively. Starting from scan 9496, all DS spectral variations are greater than 0.01. For FOV 2 (blue curves), the DS spectral variations begin to rise from

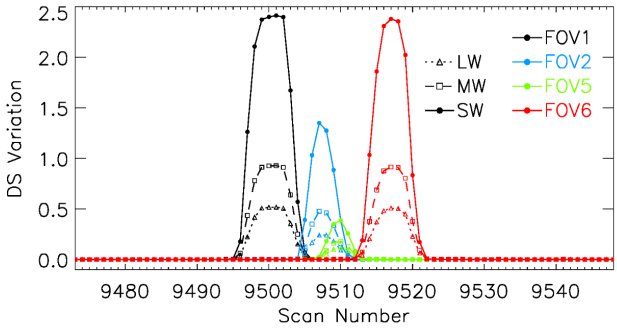

Fig. 6. Time series S-NPP CrIS reverse interferometer sweep direction DS spectral variations at FOVs 1, 2, 5, and 6 on 25 February 2018 during a lunar intrusion event. Determination of the three bands LI_{lim} values.

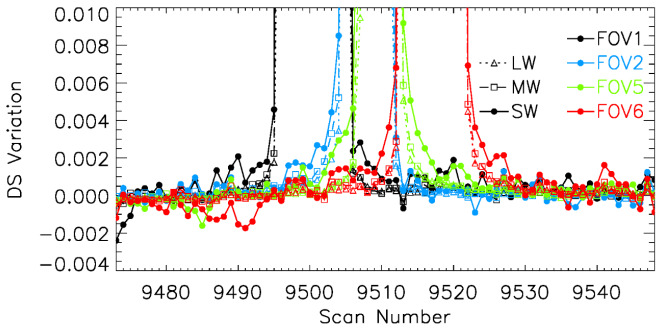

Fig. 7. Same as Fig. 6, except for zoom in, and set the DS variation range to [-0.004 to 0.01].

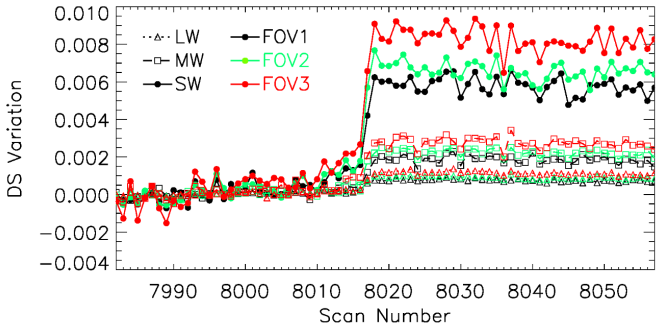

Fig. 8: Time series S-NPP CrIS forward interferometer sweep direction DS spectral variations at FOVs 1, 2, and 3 on 4 January 2019 during a non-lunar intrusion event for a false alarm case.

scan 9503 (0.002 at LWIR, 0.0035 at MWIR, and 0.0045 SWIR) and scan 9504 (0.0035 at LWIR, 0.005 at MWIR, and 0.0085 at SWIR). For FOV 5 (green curves), when lunar moves out this FOV, at scan 9513, the DS variations are at about 0.005 at LWIR, 0.006 at MWIR, and 0.009 at SWIR. For the next scan 9514, the DS variations decrease to 0.002 at LWIR, 0.003 at MWIR, and 0.005 SWIR. For FOV 6 (red curves), the DS variations are about 0.0045, 0.005, 0.007 at scan 9522, and decrease to 0.0015, 0.002, and 0.0035 for the LWIR, MWIR, and SWIR bands, respectively.

Based on previous analysis of the CrIS DS variations for all the lunar intrusion events found during the period of 2017 and 2018, for both S-NPP and NOAA-20, the thresholds LI_{lim} for the CrIS spectral bands were redefined from 0.1, for all bands, to 0.003, 0.003, and 0.0055, for the LWIR, MWIR and SWIR bands, respectively. On 17 December 2018, this new set of threshold values was implemented into the IDPS operational system Block 2.1 Mx 4, as part of the improved lunar intrusion algorithm. After this operational implementation, a number of false alarm cases (non-lunar intrusion events) were identified by the lunar intrusion quality flag QF2. Those cases were related to the tighter threshold values, especially for SW band. On a typical day with no lunar event, for NOAA-20, about ~0.2% and ~0.7% of false alarm cases were found for the MWIR and SWIR bands, respectively. For S-NPP, the false alarm cases are significantly lower than NOAA-20 with ~0.2% for SWIR. After investigating the impact on calibrated ES radiances over these false alarm cases, results indicated that the radiometric impact was very small. Essentially, radiometric errors below or near noise level were found, which should not have any meaningful impact to the downstream products. However, in some severe cases, the valid DS window size can be less than 15, resulting in degraded overall SDR quality. Further fine-tuning of the LI thresholds for different bands was performed in order to reduce the false alarm rate and improve the overall SDR data quality.

The NOAA STAR Integrated Calibration/Validation System (ICVS) was used to routinely and continuously monitor the false alarm cases after the implementation of the recent improved lunar intrusion algorithm in IDPS (https://www.star.nesdis.noaa.gov/icvs). After analyzing the quality of the CrIS SDR data, it was identified that the majority of degraded overall quality cases were associated with the false alarm lunar intrusion events that happened at descending orbits and were located at South Atlantic Anomaly (SAA) [18] regions around latitude of [-45ºS, -40ºS] during the period from December 2018 to February 2019. In general, S-NPP has more cases than NOAA-20 due to S-NPP relative larger DS spectra variation, especially at SWIR band. These cases were collected and carefully analyzed. The DS spectral variation from one of these cases on January 4, 2019 is shown in Fig. 8. It can be seen that the SWIR DS variations for all three FOVs 1, 2 and 3 exceed the threshold 0.0055 after scan 8018 with maximum value at 0.0094. The MWIR DS variations for FOV 3 also exceed the threshold 0.003. Based on these results, to effectively eliminate these false alarm cases, the thresholds LI_{lim} were optimally refined and set to [0.003, 0.004, 0.0095] for the LWIR, MWIR and SWIR bands, respectively. One of the possible reasons for this larger DS spectra variation at these SAA regions is that the very high energy SAA particles such as protons penetrate deep into the instrument shields and convert some of this kinetic energy into numerous X-rays, which can cause relative large variations to the DS, ICT, or ES views. It was found that these new set of threshold values were optimal and work for both S-NPP and NOAA-20 under current conditions with lunar phase angles within 50º to 90º (see Fig. 3). It should be pointed out that an ideal threshold should also work under different lunar phases and different instrument gains. The DS variation behavior during LI may change due to the orbit plane drift and the Moon in different phase angles. However, the orbit planes of S-NPP and NOAA-20 are controlled and stable, and the CrIS instrument gains on both satellites are very stable too, with only small degradation during mission lifetime. Both of these factors will only have very limited impact on the thresholds LI_{lim} derived in this study.

D. Implementation of the New Lunar Intrusion Detection Algorithm

An improved lunar intrusion algorithm has been developed in the operational system to effectively remove the lunar-contaminated DS spectra from the DS calibration 30-scan moving window as well as to reduce the false alarm

rate. The new thresholds LI_{lim} for three CrIS bands, LWIR, MWIR, and SWIR, are set to 0.003, 0.004 and 0.0095, respectively, which are significantly lower than the original threshold values of 0.1, implemented operationally since February 2012 (Table I). In order to obtain a high quality DS reference spectrum, the first step in the new LI algorithm is to accumulate 25 DS spectra in the moving window, and then to obtain the DS reference spectrum without the lunar contamination from these DS spectra. The 1th, 12th and 23th DS spectra magnitude were calculated and compared based on the fact that the lunar intrusion rarely affects more than 10 consecutive scans for a given FOV according to the geometric relationship between the satellite and the Moon in section III A. At least two spectra in these three selected spectra should be free of lunar contamination. To speed up the comparison, only those channels located between [864 cm^{-1}, 901 cm^{-1}], [1234 cm^{-1}, 1271 cm^{-1}], and [2184 cm^{-1}, 2222 cm^{-1}] are selected due to their strongest signal response to the instrument for CrIS LWIR, MWIR, and SWIR, respectively (see Fig. 5). The minimum magnitude difference among spectra 1th and 12th, 1th and 23th, and 12th and 23th are obtained. In this process, the first DS spectrum without lunar contamination is found in the spectral pair containing the minimum magnitude difference. With the identification of the non-contaminated DS spectrum, as an initial reference, the DS moving window can be effectively established based on the original lunar intrusion algorithm with the new thresholds. The new threshold values guarantee that all the DS spectra in the moving window are free of the lunar contamination. One of the major advantages of the improved CrIS LI algorithm is related to its computational efficiency, making it applicable to all DS spectra without meaningful impact on the latency. Therefore, there is no need to implement a prediction model for forecasting the presence of potential lunar intrusion events before applying this new algorithm, which would imply significant code changes in the operational system. Table I summarize the improvements of the new lunar intrusion detection algorithm compared to the first operational algorithm in terms of threshold and code changes.

IV. Results

To evaluate the new lunar intrusion algorithm, we generated offline SDR data using the new lunar intrusion algorithm for lunar intrusion events with two running settings: serial and parallel processing. For the serial mode, all CrIS RDR granule data (each granule includes 4 scans) are processed in a sequential fashion without reinitializing the first-in-first-out DS

TABLE I
IMPROVEMENTS OF THE NEW LUNAR INTRUSION DETECTION ALGORITHM

Algorithm	Implementation Date	Code Main Feature	Threshold		
			LWIR	MWIR	SWIR
Original LI Detection Algorithm	From February 2012 until 17 December 2018	Assuming the first DS spectrum in the moving window was non-contaminated as initial reference spectrum	0.1	0.1	0.1
New LI detection algorithm	17 December 2018 IDPS Block 2.1 Mx 4	Finding a non-contaminated spectrum in the moving window to use as the initial reference spectrum	0.003	0.003	0.0055
New LI detection algorithm with improved LI thresholds	10 May 2019 IDPS Block 2.1 Mx 5	Finding a non-contaminated spectrum in the moving window to use as the initial reference spectrum	0.003	0.004	0.0095

(a) LWIR band

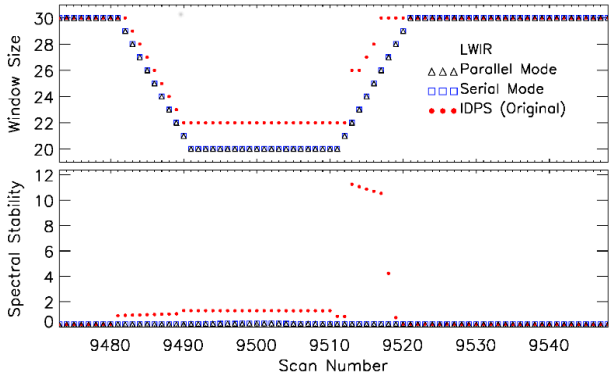

(b) MWIR band

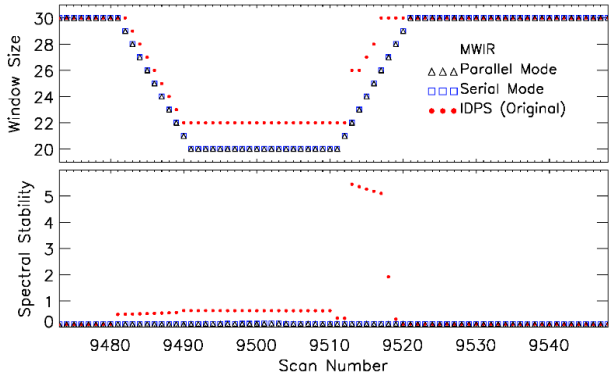

(c) SWIR band

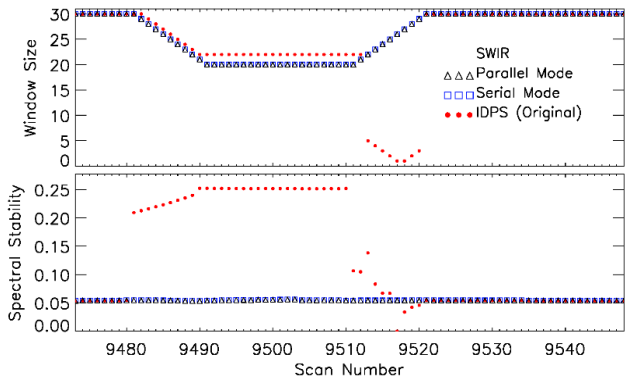

Fig. 9. DS moving window size and spectral stability as a function of scan lines in a lunar intrusion event on 25 February 2018 for S-NPP CrIS reverse sweep direction at FOV 1 for three CrIS bands (a) LWIR band (b) MWIR band, and (c) SWIR band. The serial mode (blue square) can be treated as truth since DS moving window does not need to be reestablished and the first DS spectrum is contamination-free. IDPS (red filled circle) is referred to the original operational algorithm before 17 December 2108 with lunar intrusion threshold as 0.1 for all three bands, while parallel mode (black triangle) is for the new algorithm. Both serial mode and parallel mode are using new threshold values as 0.003, 0.004, and 0.0095 for three CrIS bands, respectively.

30-scan moving window for each new granule of SDR. While for the parallel mode, which mimics the IDPS operational environment, each granule of SDR is independently generated from 9 consecutive granules of RDRs (to include at least 34 scans ICT and DS spectra to calibrate the 4 scans ES spectra) after initializing its own DS moving window. The SDR data generated from the serial mode is treated as reference in this study since the ES spectra are always calibrated with non-contaminated DS reference spectrum. All the lunar intrusion events from January 2017 to April 2018 were tested and successfully detected using the new lunar intrusion algorithm with the two new sets of derived thresholds, shown in Table I, implemented in our offline calibration system and has been implemented operationally in IDPS processing system since 17 December 2018 and 10 May 2019, respectively. In this work, a representative LI event on 25 February 2018 is presented.

A. DS Calibration Moving Window Size and DS Spectral Stability

The comparison results for the DS calibration moving window size and DS spectral stability from the SDR data generated from the original LI algorithm in IDPS and those generated from the new lunar intrusion algorithm are shown in Fig. 9. In this figure, the DS moving window size and spectral stability are plotted as a function of scan lines in a lunar intrusion event on 25 February 2018 for S-NPP CrIS reverse sweep direction at FOV 1. The serial mode (blue square) can be treated as truth since DS moving window does not need to be reestablished for each SDR granule. The IDPS result (red filled circle) is referred to the original operational algorithm before 17 December 2018 with lunar intrusion threshold set to 0.1 for all three bands, while parallel mode (black triangle) is for the new algorithm. Both serial mode and parallel mode are using new threshold values as 0.003, 0.004, and 0.0095 for three CrIS bands, respectively. The IDPS is basically run in parallel mode after IDPS Block 2.0 Mx 0, which was implemented into operations on 8 March 2017. After that day and during a lunar intrusion event, a lunar intrusion anomaly showed up with degraded and invalided CrIS SDR overall quality, indicated by the quality flag QF3, and was caused by the DS moving window size less than 15 or imaginary radiance exceeding the prescribed threshold, especially for SWIR band.

A detailed description of how the LI detect algorithm handles the lunar-contaminated DS spectra in serial run is given below, with support from results found in Fig. 9. For the serial run, when SDR granule containing scan number from 9481 to 9484 is produced, the DS moving window includes 30-scan non-contaminated DS spectra (from scan 9466 to 9495) to calibrate the ES spectra at scan number 9481 (corresponding the 16th scan in the 30-scan moving window). For the next scan 9482, DS spectrum at scan 9496 is pushed into the moving window, and at the same time DS spectrum at scan 9466 is popped out of the moving window. Since DS spectrum at scan 9496 is contaminated by lunar radiation (see Fig. 7), it is rejected due to the DS spectrum variation exceeding the threshold and not included in the calculation of the DS reference spectrum, resulting in DS window size of 29 used for the calibration of the ES spectra at scan 9482. Following that, the DS window size for ES spectra at scan 9483 should be 28 since the last DS spectrum at scan 9497 is contaminated by lunar radiation and rejected from the moving window and the non-contaminated DS spectrum at scan 9467 popping out. As such, the DS window size is gradually reduced by one until 20 at scan 9491 (there is a total of 10 lunar-contaminated DS spectra from scan 9496 to 9505 that are rejected). The DS window size maintains at 20 until scan 9511 since all of DS spectra after scan 9505 are normal and replace these first-in normal DS spectra in the 30-scan moving window. At scan 9511, the DS moving window keeps 20 scans with non-contaminated DS spectra from scan 9506 to 9525, and reject the first 10 scans from 9496 to 9505 to calibrate the ES spectra. For the next 10 scans ES spectra until 9521, the DS calibration window size will be gradually increased by one since one more normal DS spectrum is pushed into the moving window. After scan 9521, all ES spectra are calibrated with DS reference spectrum averaged from 30 lunar-contamination-free DS spectra. One can see from Fig. 9, the DS moving window size as a function of scans are consistent among three CrIS bands and gradually decreasing/increasing as the Moon moving in and out from the FOV in the serial run (blue square). In addition, the DS spectral stability before, during, and after the lunar intrusion event are at the same level as a function of scans for each band. These results clearly demonstrate that the new lunar intrusion algorithm works successfully to detect and reject those lunar-contaminated DS spectra during the calculation of the DS reference spectrum within the moving window.

For the parallel run, each process independently establishes its own calibration moving windows for ICT and DS spectra to generate one granule of SDR. The results from the parallel run (black triangle) are essentially the same as the serial run. There is no noticeable difference between these runs in terms

of DS moving window size and DS spectral stability. This clearly shows that the new LI detection algorithm would work well in the operational environment for parallel run.

The results from the original LI detection algorithm (red circle) showed that it failed to effectively detect and reject the lunar-contaminated DS spectra. As a result, the DS calibration window size is not consistent among different bands and jump down and up along the scans. For example, one granule generated by IDPS, which includes four scans from 9517 to 9520, has DS window sizes at three bands [LWIR, MWIR, SWIR] with [30, 30, 1], [30, 30, 1], [30, 30, 2], [30, 30, 3], respectively. In this case, the original algorithm in the parallel IDPS process used the first DS spectrum at scan 9502 as an initial DS reference spectrum to sequentially establish the 30-scan DS moving window for each band. However, this DS spectrum at scan 9502 is strongly contaminated by lunar radiation (see Fig. 6). Consequently, all the next 29 DS spectra in the SWIR band are rejected, resulting in a DS calibration window size of 1 to calibrate the ES spectra at scan 9517. As a result, the SWIR overall data quality flags at the FOV1 reverse sweep direction for the all 4 scans ES spectra in this SDR granule are set to "degraded" status, due to the DS calibration window sizes of [1, 1, 2, 3] less than 15. For MWIR and LWIR bands, due to the high threshold values used in the original LI detection algorithm, there were no lunar-contaminated DS spectra rejected from the moving window. In addition, the lunar-contaminated DS spectra were included in the DS calibration moving window for the original algorithm. This can be clearly seen from the larger variation of the DS spectral stability as a function of scans. The DS spectral stability changed dramatically as a function of scans for all three bands whenever there are lunar-contaminated spectra included in the DS moving window from scan 9481 to scan 9520. Typically, this data quality indicator is more sensitive to the SWIR band due to the larger spectra magnitude changes resulted from lunar radiation. This DQI is a very good indicator to show whether the LI detection algorithm works well or not.

B. Impacts on ES Radiances and Data Quality

As one of two essential calibration references, DS view measurements' stability and accuracy are critical for calibrating the Earth scene spectra and radiances. Due to the larger lunar intrusion threshold values and incorrect DS reference spectrum in the original algorithm, the calibration error is introduced for the ES spectra during the lunar intrusion events. Prior to the implementation of IDPS Block 2.0 Mx 0 (8 March 2017), the operational system ran in a serial mode, and there were no SDR ES spectra with overall quality flag QF3 triggered as degraded or invalid during lunar intrusion events due to the small DS calibration window size. Once the IDPS Block 2.0 Mx 0 became operational, the overall quality flag QF3 triggered as degraded or invalid were often observed during lunar intrusion events, especially for SWIR band. One can observe that the DS spectral stability significantly increased up during lunar intrusion events as seen from the ICVS monitoring website (https://www.star.nesdis.noaa.gov/icvs), which indicated that the lunar-contaminated DS spectra were included in the calibration moving window to calculate the DS reference spectrum. As a result, the ES spectra calibrated with the contaminated DS reference spectrum were subject to calibration error.

Figure 10(a)-(c) shows the brightness temperatures (BT) from serial run as references, BT differences for these two parallel runs (one for the original and one for the new LI detection algorithm) compared to the serial run for these FOVs affected by lunar intrusion at three wavenumbers: 900.0 cm^{-1}, 1252.50 cm^{-1}, and 2203.125 cm^{-1}, respectively, on a lunar intrusion event on 25 February 2018. The observed BTs from these three channels have large dynamic ranges, and have high contrast over clear-sky and over clouds. Therefore, they are very suitable to evaluate the effect of lunar contamination in the DS reference spectrum on the ES spectra. It can be seen that the

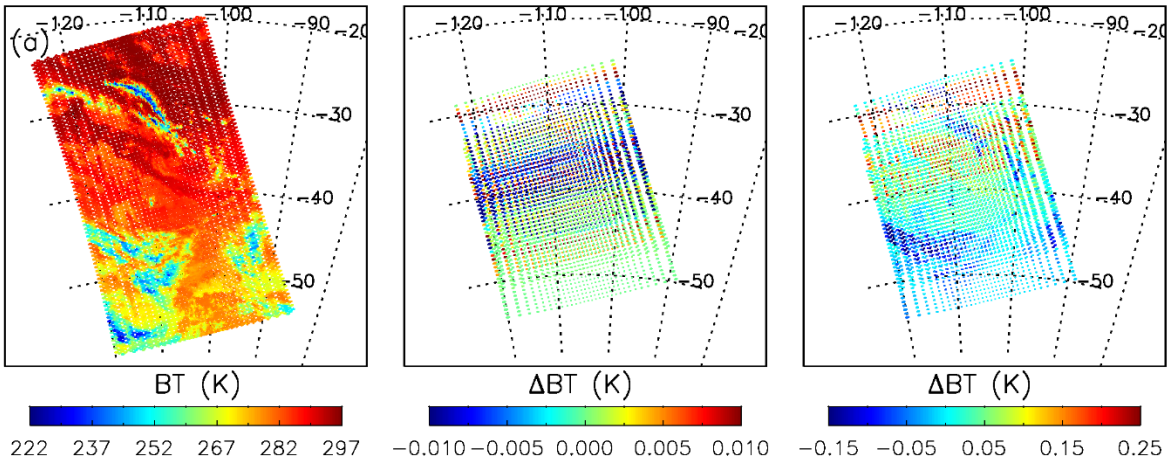

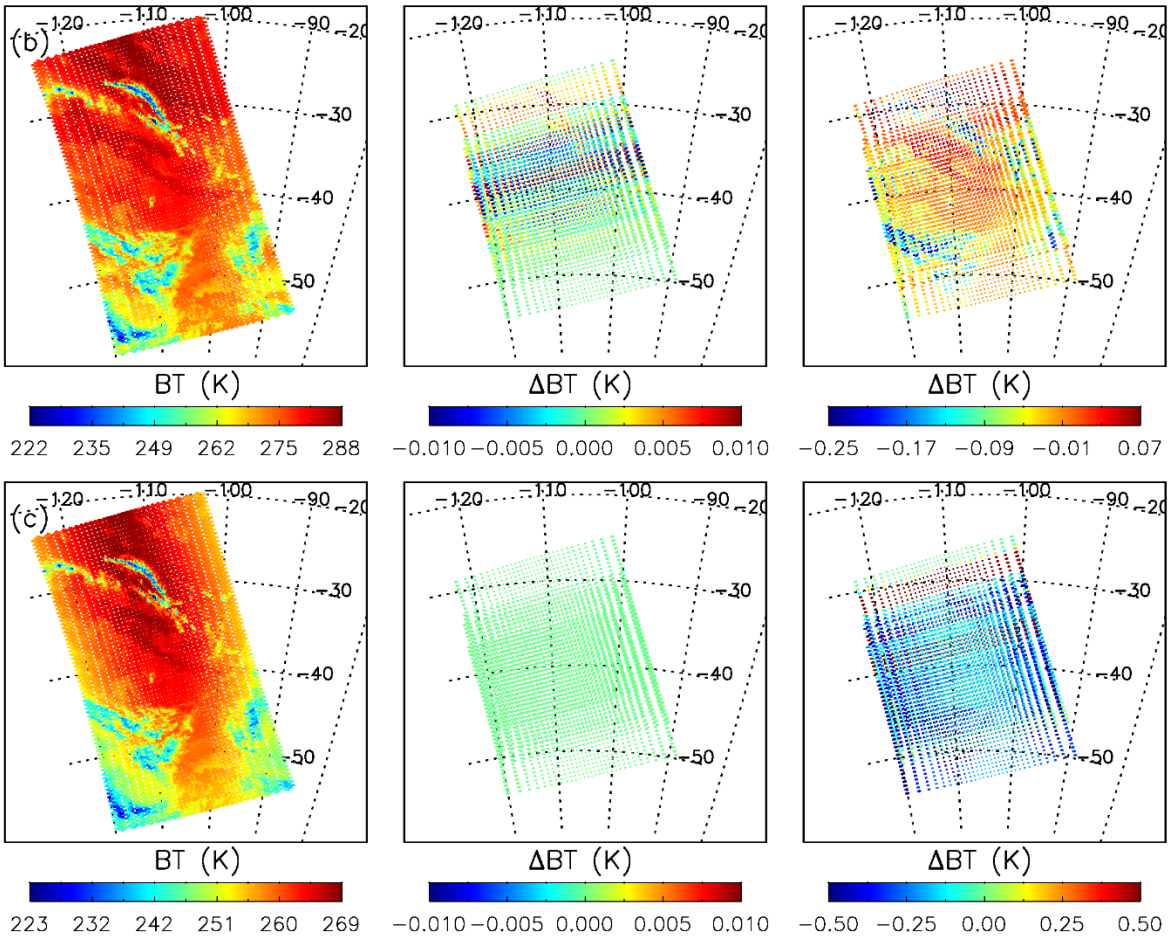

Fig. 10. Brightness temperatures (BT) from serial run as references (left column), and BT differences for these two parallel runs compared to the serial run (middle column: BT difference between the parallel run and the serial run using new LI detection algorithm, and last column: BT difference between the original and new LI detection algorithms) for these FOVs affected by lunar intrusion at three wavenumbers: (a) 900.0 cm^{-1}, (b) 1252.50 cm^{-1}, and (c) 2203.125cm^{-1}, respectively, on a lunar intrusion event on 25 February 2018.

BT differences from the middle column (difference between the parallel run and the serial run using the new LI detection algorithm) are negligible (ranging from -0.01 to 0.01 K). The difference mainly come from the digital rounding error when calculating the DS reference spectrum in different running settings. However, the BT differences from the last column (difference between the original and new LI detection algorithms) are clearly noticeable with the differences range from -0.15 K to 0.25 K (LWIR), from -0.25 K to 0.07 K (MWIR), and from -0.5 K to 0.5 K (SWIR). These BT differences would negatively impact downstream products as well as weather applications such as direct assimilation into numerical weather prediction models and climate applications. The BT differences are also scene dependent especially for LWIR channel and MWIR channel. The BT difference at SWIR can reach hundred K due to the very small DS calibration window size and highly distorted DS reference spectrum (for displaying purpose, not shown in this figure).

Due to the temporal and spatial coverage of the lunar intrusion events for CrIS observation, as well as the significant improvements on ES radiances and SDR data quality, the new lunar intrusion detection algorithm with threshold values LI_{lim} as [0.003, 0.003, 0.0055] for the LWIR, MWIR, and SWIR respectively, were operationally implemented on IDPS Block 2.1 Mx 4 on 17 December 2018. The new algorithm shows a successful detection and removal of all the lunar-contaminated DS spectra in the DS moving window, and resulting in better and accurate calibrated ES radiances during lunar intrusion events. However, some false alarm cases, in which the quality flag QF2 were triggered due to the very tight thresholds, during non-lunar intrusion events were observed. To effectively eliminate these false alarms, a new set of optimal thresholds values, LI_{lim}, were derive and properly validated using our offline calibration system. Final threshold values were implemented operationally on 10 May 2019 in IDPS Block 2.1 Mx 5 with [0.003, 0.004, 0.0095] for the LWIR, MWIR, and SWIR bands, respectively.

V. CONCLUSION

As one of the calibration reference targets, the stable DS reference spectrum in the moving window is critically important for the accuracy of the calibrated ES radiances. The raw DS spectrum changes when the lunar radiation intrudes into the observation FOV. The original LI detection algorithm

in IDPS system did not consistently remove the lunar-contaminated DS spectra from the DS moving window due to the larger threshold values (0.1 for all three bands) and the assumption that DS spectrum of the first scan in the moving window is contamination-free. As a result, IDPS sometimes produced inaccurate, degraded, or invalid ES radiances in the SDR data product during lunar intrusion events. In this study, a new improved LI detection algorithm has been developed and implemented into the IDPS operational system since 17 December 2018. First, the new algorithm efficiently finds a non-contaminated DS spectrum in the 30-scan calibration moving window to use as the reference spectrum since the lunar intrusion rarely affects more than 10 scans of DS views for a given FOV. Second, based on the phase characteristics of the complex raw DS spectra during LI events, the new lunar intrusion band-dependent thresholds [0.003, 0.003, 0.0055] were derived to effectively reject the contaminated DS spectra and make the valid DS window size consistent among the three bands.

The new algorithm and thresholds implemented in the IDPS system show a successful detection and removal of all the lunar-contaminated DS spectra in the DS moving window, resulting in more accurately calibrated ES radiances during lunar intrusion events. To effectively eliminate some false alarms on non-lunar intrusion events, the thresholds LI_{lim} were optimally raised to [0.003, 0.004, 0.0095] from [0.003, 0.003, 0.0055] for LWIR, MWIR and SWIR bands, respectively. The new algorithm with the optimal thresholds was validated in our offline SDR processing system and went operationally on 10 May 2019 in IDPS processing system. The calibration error in the original algorithm are on the order of several tenths of a K in all three CrIS bands, and could negatively impact downstream products as well as weather and climate applications. Compared to the original LI detection algorithm, the new algorithm significantly improves the SDR data quality and the accuracy of the calibrated ES spectra, reducing errors during LI events to 10 mK or less.

This new LI algorithm can be applicable to the CrIS instrument on the future JPSS satellites (J2 to J4) since those satellites will operate at the same orbit plane. The method to determine the LI optimal threshold values, which were used to effectively remove the lunar contaminated DS view measurement, can be used for the future CrIS instrument and similar FTS instruments such as the Infrared Atmospheric Sounding Interferometer (IASI) on the European MetOp satellite series and the Hyper-spectra Infrared Atmospheric Sounder (HIRAS) on the FY-3D satellite.

Acknowledgment

The authors thank Drs. Wenhui Wang and Hu Yang as well as two anonymous reviewers for providing constructive comments to improve this paper. The contents of this paper are solely the opinions of the authors and do not constitute a statement of policy, decision, or position on behalf of NOAA or the U.S. Government.

References

[1] Y. Han, H. Revercomb, M. Cromp, D. G. Gu, D. Johnson, D. Mooney, et al., “Suomi NPP CrIS measurements, sensor data record algorithm, calibration and validation activities, and record data quality,” Journal of Geophysical Research-Atmospheres, vol. 118, pp. 12734-12748, Nov 27 2013.

[2] D. Tobin, H. Revercomb, R. Knuteson, J. Taylor, F. Best, L. Borg, et al., “Suomi-NPP CrIS radiometric calibration uncertainty,” Journal of Geophysical Research: Atmospheres, vol. 118, pp. 10,589-10,600, 2013.

[3] L. L. Strow, H. Motteler, D. Tobin, H. Revercomb, S. Hannon, H. Buijs, et al., "Spectral calibration and validation of the Cross-track Infrared Sounder on the Suomi NPP satellite," Journal of Geophysical Research-Atmospheres, vol. 118, pp. 12486-12496, Nov 27 2013.

[4] L. Wang, D. A. Tremblay, Y. Han, M. Esplin, D. E. Hagan, J. Predina, et al., "Geolocation assessment for CrIS sensor data records," Journal of Geophysical Research-Atmospheres, vol. 118, pp. 12690-12704, Nov 27 2013.

[5] V. Zavyalov, M. Esplin, D. Scott, B. Esplin, G. Bingham, E. Hoffman, et al., "Noise performance of the CrIS instrument," Journal of Geophysical Research-Atmospheres, vol. 118, pp. 13108-13120, Dec 2013.

[6] Y. Chen, F. Weng, and Y. Han, "SI traceable algorithm for characterizing hyperspectral infrared sounder CrIS noise," Appl. Opt., vol. 54, pp. 7889–7894, 2015.

[7] Y. Chen, Y. Han, and F. Weng, "Characterization of long-term stability of Suomi NPP Cross-Track Infrared Sounder spectral calibration," IEEE Transactions on Geoscience and Remote Sensing, vol. 55, No. 2, pp. 1147-1159, Feb. 2017.

[8] Y. Chen, Y. Han, and F. Weng, “Reprocessing of Suomi NPP CrIS sensor data records and impacts on radiometric and spectral long-term accuracy and stability,” in Proc. IEEE International Geoscience and Remote Sensing Symposium, Jul. 2017, pp. 4178-4181.

[9] L. Wang, B. Zhang, D. Tremblay, and Y. Han, "Improved scheme for Cross-track Infrared Sounder geolocation assessment and optimization," Journal of Geophysical Research-Atmospheres, vol. 121, doi:10.1002/2016JD025812, 2016.

[10] R. Eresmaa, J. Letertre-Danczak, C. Lupu, N. Bormann, and A. P. McNally, “The assimilation of Cross-track Infrared Sounder radiances at ECMWF,” Quarterly Journal of the Royal Meteorological Society, vol. 143, no. 709, pp. 3177-3188, 2017.

[11] N. Smith, W. L. Smith, E. Weisz, and H. E. Revercomb, “AIRS, IASI, and CrIS Retrieval Records at Climate Scales: An Investigation into the Propagation of Systematic Uncertainty,” Journal of Applied Meteorology and Climatology, vol. 54, pp. 1465-1481, Jul 2015.

[12] C. Cao, Y. Chen, X. Jin, D. Tremblay, A. Wald, S. Kireev, L. Wang, “Cross Track Infrared Sounder (CrIS) Sensor Data Record (SDR) User’s Guide,” Version 1.1, April

2018. [Available online at https://www.star.nesdis.noaa.gov/jpss/documents/UserGuides/CrIS_SDR_Users_Guide1p1_20180405.pdf]

[13]H. Revercomb, H. Buijs, H. B. Howell, D. D. LaPorte, W. L. Smith, and L. A. Sromovsky, "Radiometric calibration of IR Fourier transform spectrometers: Solution to a problem with the High-Resolution Interferometer Sounder," Applied Optics, pp. 273210-273218, 1988.

[14]J. Bangert, W. Puatua, G. Kaplan, J. Bartlett, W. Harris, A. Fredericks, and A. Monet, "User's Guide to NOVAS Version C3.1," U.S. Nav. Obs, Washington, D. C., 2011.

[15]W. M. Folkner, Williams, J.G., Boggs, D.H., "The Planetary and Lunar Ephemeris DE 421," IPN Progress Report 42-178, August 15 2009. [Available online at http://ipnpr.jpl.nasa.gov/progress_report/42-178/178C.pdf]

[16]N. Z. Miura, "Comparison and design of Simplified General Perturbation Models (SGP4) and code for NASA Johnson Space Center," ORBITAL DEBRIS PROGRAM OFFICE. PhD thesis, Faculty of California Polytechnic State University, 2009. [Available online at https://digitalcommons.calpoly.edu/theses/86/]

[17]JPSS Configuration Management Office, "Joint Polar Satellite System (JPSS) Cross Track Infrared Sounder (CrIS) Sensor Data Records (SDR) algorithm theoretical basis document (ATBD) for normal spectral resolution", JPSS office, document code D0001-M01-S002, June 2018. [Available online at https://www.star.nesdis.noaa.gov/jpss/documents/ATBD/D0001-M01-S01-002_JPSS_ATBD_CRIS-SDR_nsr_20180614.pdf]

[18] F. Pavón-Carrasco, and A. De Santis, "The South Atlantic Anomaly: The Key for a Possible Geomagnetic Reversal," Frontiers in Earth Science, vol. 4, 40, https://doi.org/10.3389/feart.2016.00040, April 2016.

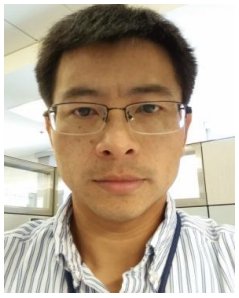

Yong Chen received the B.S. and M.S. degree in atmospheric sciences from Peking University, Beijing, China, in 1996 and 1999, respectively, and the Ph.D. degree in atmospheric sciences from University of California, Los Angeles, in 2006.

From 2006 to 2013, he was a research scientist with the Cooperative Institute for Research in the Atmosphere, Colorado State University. From 2013 to 2019, he was a research scientist with Earth System Science Interdisciplinary Research Center, University of Maryland at College Park. Current, he is a senior scientist at Global Science and Technology, Inc., Greenbelt, Maryland. The major fields that he is working on include the following: 1) Radiative transfer theory and applications; 2) Development and implementation of fast radiative transfer model for satellite data assimilation; 3) Radiometric and spectral calibration and validation of satellite hyper-spectral infrared sounder.

Denis Tremblay received the Ph.D. degree in aerospace engineering from the University of Colorado, Boulder, in 1995. He has been a member of the CrIS team since 2006. He contributed to the software development with emphasis on the calibration (SDR), geolocation, simulation, integration, testing, and science validation.

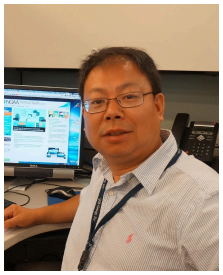

Likun Wang received the B.S. degree in atmospheric sciences and the M.S. degree in meteorology from Peking University, Beijing, China, in 1996 and 1999, respectively, and the Ph.D. degree in atmospheric sciences from University of Alaska Fairbanks, in 2004. He is now working in NOAA/NESDIS/STAR as a contract scientist employed by Riverside Technology Inc. for near space payload hosting platform assessment (such as Google Loon) and artificial intelligence for satellite application. He currently also serves the chair of World Meteorological Organization (WMO) sponsored Global Space-based Inter-Calibration System (GSICS) infrared sensor working group.

Flavio Iturbide-Sanchez (S'03–M'07–SM'19) received the B.S.E.E degree in electronics engineering from Autonomous Metropolitan University, Mexico City, Mexico, in 1999, the M.S.E.E. degree in electrical engineering from the Advanced Studies and Research Center, National Polytechnic Institute, Mexico City, in 2001, and the Ph.D. degree from the University of Massachusetts, Amherst, MA, USA, in 2007, where he was advised by Prof. S. C. Reising and supported by the National Science Foundation.

His Ph.D. research focused on the miniaturization, development, calibration, and performance assessment of low-cost and power-efficient microwave radiometers for remote sensing applications. From 2001 to 2005, he was a Research Assistant with the Microwave Remote Sensing Laboratory, University of Massachusetts, where he was involved in the design, development, and characterization of highly integrated multichip modules and microwave circuits for low-noise, low-power consumption, high-gain, and high-stability microwave radiometers. From 2005 to 2007, he was with the Microwave Systems Laboratory, Colorado State University, Fort Collins, CO, USA, focusing on development, characterization, calibration, and deployment of the low-cost and power-efficient compact microwave radiometer for humidity profiling. From 2008 to 2018, he was with the I. M. Systems Group, Inc., supporting the development of operational physical retrieval systems that employ

hyperspectral-infrared and microwave observations implemented for the NOAA Polar Operational Environmental Satellites Project, the National Polar-orbiting Operational Environmental Satellite System, and the Joint Polar Satellite System (JPSS). He has been a Physical Scientist with NOAA/NESDIS/Center for Satellite Applications and Research, College Park, MD, USA, since 2018, where he has led the calibration and validation of the JPSS Cross-track Infrared Sounder instruments. His research interests include satellite remote sensing, satellite data assimilation, inverse theory applied to geoscience fields, weather forecasting, earth system science, small satellites, and the design of radiometer systems for earth observations based on emerging technologies.

Dr. Iturbide-Sanchez was a recipient of the First-Place Poster Award at the 11th Specialist Meeting on Microwave Radiometry and Remote Sensing Applications (MicroRad 2010), Washington, DC, USA, and the Mexican National Council for Science and Technology Graduate Fellowship from 1999 to 2004. He was a Finalist in two IEEE Student Paper Competitions, one at the International Geoscience and Remote Sensing Symposium in Anchorage, AK, USA, in 2004 and one at the International Microwave Symposium in San Francisco, CA, USA, in 2006.